

Robust Iris Segmentation Based on Learned Boundary Detectors

Haiqing Li, Zhenan Sun and Tieniu Tan

National Laboratory of Pattern Recognition

Institute of Automation, Chinese Academy of Sciences, Beijing, P.R. China, 100190

{hqli, znsun, tnt}@nlpr.ia.ac.cn

Abstract

Iris segmentation aims to isolate the valid iris texture regions useful for personal identification from the background of an iris image. Most state-of-the-art iris segmentation methods are based on edge information. However, generic edge detection methods may generate a large number of noisy edge points which can mislead iris localization. Therefore a robust iris segmentation method based on specific edge detectors is proposed in this paper. Firstly, a set of visual features including intensity, gradient, texture and structure information is used to characterize the edge points on iris boundaries. Secondly, AdaBoost is employed to learn six class-specific boundary detectors for localization of left/right pupillary boundaries, left/right limbic boundaries and upper/lower eyelids respectively. Thirdly, inner and outer boundaries of the iris ring are localized using weighted Hough transforms based on the output of the corresponding detectors. Finally, the edge points on the eyelids are detected and fitted as parabolas by robust least squares fitting. Extensive experiments on the challenging CASIA-Iris-Thousand iris image database demonstrate the effectiveness of the proposed iris segmentation method.

1. Introduction

Iris images usually contain not only iris texture regions useful for identity verification but also the neighboring background regions such as pupil, sclera, and eyelids. So iris segmentation is necessary to isolate the valid iris regions from the background for iris pattern analysis and recognition. Although iris segmentation is important to iris recognition, it has become a bottleneck of iris recognition due to the following reasons: 1) It is difficult to detect the boundaries of iris rings due to intensity variations of iris images, occlusions of eyelids and eyelashes and specular reflections. As shown in Figure 1, various noises (such as eyeglass frames, specular reflections, eyelids and eyelashes occlusions, etc.) in iris images are grand challenges for accurate iris segmentation; 2) Iris segmentation is the most compu-

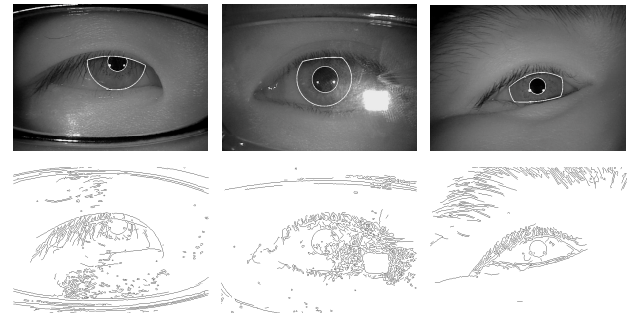


Figure 1. Top Row: Examples of segmentation results by the proposed method on various challenging iris images which are from CASIA-Iris-Thousand database [1]; Bottom Row: Edges detected by Canny edge detectors.

tationally expensive procedure in iris recognition owing to the complexity of computer vision algorithms for iris segmentation.

Iris segmentation is a hot research topic of iris recognition. There are two typical methods for iris segmentation which are proposed by Daugman and Wildes respectively. Daugman [4] used Integrodifferential operators as circular edge detectors to fit inner and outer boundaries. His later work [5] also used Integrodifferential operators to detect curvilinear eyelids boundaries. Wildes [18] created a binary edge-map via gradient based edge detection at first and then localized the boundaries by Hough transforms.

Both the iris segmentation methods developed by Daugman and Wildes are based on the assumption of sharp intensity variations on iris boundaries. The basic idea is to find the edge points in an iris image and then use a circle model to fit these points. It means the low level visual cues of an iris image, *i.e.* edge information are important for iris segmentation. These methods tend to obtain incorrect localization results in the presence of a large number of noisy edge points or low-contrast boundaries. As Figure 1 illustrates, many noises are with high gradient but the genuine limbic boundaries are blurry in practical applications. Therefore, reliable boundary detection becomes the focus of iris segmentation and many researchers have paid much attention

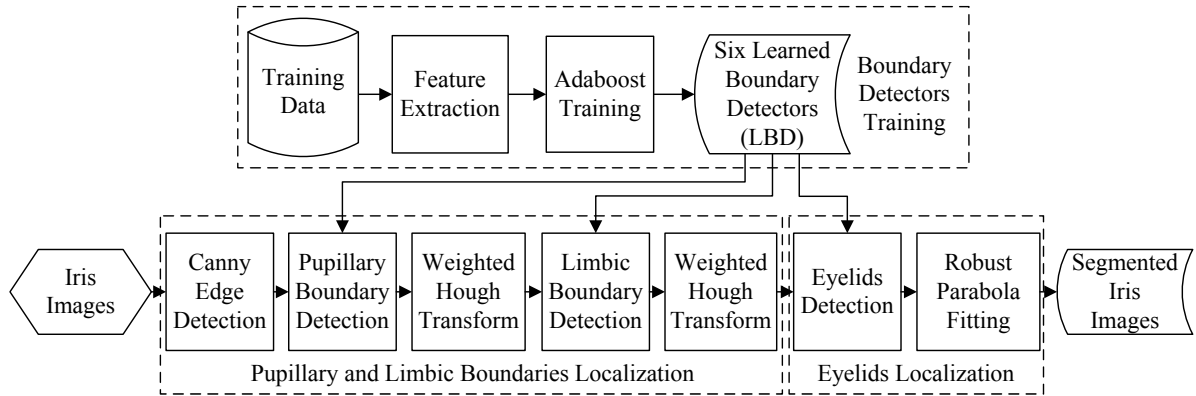


Figure 2. The flowchart of the proposed iris segmentation method.

to reduce impacts of noises. Liu *et al.* [11] used intensity thresholds to select candidate edge points. He *et al.* [8] detected pupillary and limbic edge points in polar coordinates and used histogram filtering before eyelids boundaries fitting to rule out noisy points. Liu *et al.* [12] presented a RANSAC-like algorithm to exclude invalid points. While some researchers did not only use gradient to get boundary information, Tang and Weng [16] trained a SVM classifier for limbic boundary detection using gradient and shape features. In [13], Proença and Alexandre detected edges not in original but in clustered images to create more accurate edge maps. Recently, active contours have been employed to iris segmentation without modeling boundaries as parametric curves [14, 19], which also depend heavily on edge information.

Edge information is critical for many computer vision problems and many general edge detectors have been developed [2, 3]. Such detectors can achieve good performance for general purposes, but they do not work efficiently for some specific applications [6, 9]. Then the class-specific boundary detectors are required, which have been developed in the past few years and achieved encouraging performance [6, 9, 15]. The detectors are trained by machine learning methods driven by labeled samples.

Inspired by the above referred work, we propose a robust iris segmentation method based on Learned Boundary Detectors (LBD for short). The flowchart of the proposed method is shown in Figure 2. It includes three main modules, namely, boundary detectors training, pupillary and limbic boundaries localization and eyelids localization. At first, we train six boundary detectors for left/right pupillary boundaries, left/right limbic boundaries and upper/lower eyelids by Gentle AdaBoost [7]. Then, pupillary and limbic boundaries are localized successively using weighted Hough transforms based on the output of LBD. At last, edge points of upper and lower eyelids are detected by LBD and fitted as parabolas via robust least squares fitting.

2. Technical details

2.1. Boundary detectors training

To determine whether a pixel is a specific boundary or not, a large image patch centered at the pixel is considered to take into account multiple scales information. Then a classifier is trained from labeled samples using features extracted from the image patch [6].

In order to discriminate genuine edge points on iris boundaries from noisy edge points, it is necessary to define visual features specific to iris boundaries. Intensities, edges, textures and structures are useful features for iris boundary description. Considering both discriminative abilities and computational cost, we choose mean, variance and haar-like [10] features at multiple locations, scales and aspect ratios. They are all extracted in three kinds of images, namely, gray images, gradient images in the horizontal and vertical directions. Mean values of gray and gradient contain information of intensities and edges. Variance measures textures generally while haar-like features describe structures. All these features can be calculated efficiently in integral images. More than 10,000 features are calculated in each image patch, which provides an over-complete feature set for learning.

Boosting is one of the most popular methods for feature selection and classifier construction. We choose Gentle AdaBoost [7] to construct a strong classifier for boundary detection, because it uses adaptive Newton steps in optimization and often outperforms other boosting variants, especially when noises exist in the training data. Given N training data $(x_1, y_1), \dots, (x_n, y_n), \dots, (x_N, y_N)$ with x a K dimensional feature vector and $y_n = \pm 1$. The weak classifier we used for the k -th feature is:

$$f(x^k) = a^k \delta(x^k > \theta^k) + b^k, \quad (1)$$

where parameters (a^k, b^k, θ^k) can be determined by mini-

mizing weighted square error [17]:

$$\min_{a^k, b^k, \theta^k} \sum_{n=1}^N w_n (y_n - f(x_n^k))^2, \quad (2)$$

$$b^k = \frac{\sum_n w_n y_n \delta(x_n^k \leq \theta^k)}{\sum_n w_n \delta(x_n^k \leq \theta^k)}, \quad (3)$$

$$a^k + b^k = \frac{\sum_n w_n y_n \delta(x_n^k > \theta^k)}{\sum_n w_n \delta(x_n^k > \theta^k)}, \quad (4)$$

where w_n is the weight for the n -th training sample. After M rounds, a strong classifier is constructed:

$$\text{sign}[F(x)] = \text{sign}\left[\sum_{m=1}^M f_m(x)\right]. \quad (5)$$

The learned strong classifiers will be used as boundary detectors in the following iris segmentation procedures. Settings and results of the training will be detailed in Section 3.

2.2. Pupillary and limbic boundaries localization

In near infrared iris images, pupillary boundaries usually have higher contrast than limbic boundaries and can be detected by general edge detectors. Therefore, we first use the Canny edge detector to find the pupillary candidate edge points. Along with valid pupillary boundary edge points, many invalid points will also be included due to noises. Then the previously learned left and right pupillary detectors are used to find out the genuine pupillary boundary edge points. Points with nonpositive detection scores $F(x)$ (Equation 5) will be excluded in the later step. Moreover, positive $F(x)$ can be regarded as confidence of a point to be the valid points.

Pupillary and limbic boundaries are modeled as circles and their parameters are determined by weighted Hough transforms. The Hough transform used in traditional iris segmentation treats every vote equally. In our case, we use $F(x)$ as the weight of a vote. This can increase the contributions of better valid points and then get more robust results. As we have known the left and right pupillary points, we can constrain voting angle ranges by restricting the left points only vote to centers on its right and vice versa. The angle ranges constraints can reduce not only the Hough space to search but also the impacts caused by noises.

Limbic boundary is localized in a similar way after pupillary localization. The main differences are: 1) Candidate edge points are sampled in the regions depending on the center and radius of the pupil, not on Canny detected edges; 2) Voting angle ranges are more tightly restricted

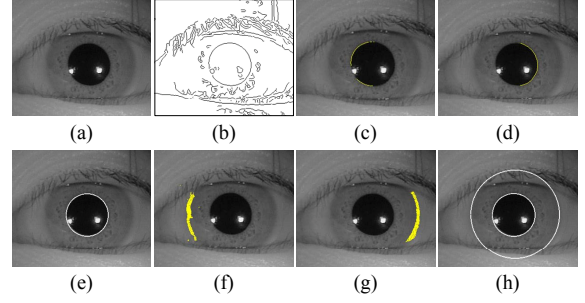


Figure 3. Intermediate results in pupillary and limbic boundaries localization (better viewed in color). (a) Original iris image; (b) Canny edge image; (c), (d), (f), (g) Yellow pixels are detected by learned left pupillary, right pupillary, left limbic and right limbic boundary detectors respectively; (e), (h) Pupillary and limbic boundaries fitted as circles by weighted Hough transforms.

since a limbic boundary center should be near to the pupillary center.

Figure 3 shows some intermediate results in pupillary and limbic boundaries localization. Genuine boundary points have been detected by the learned boundary detectors and most of noisy points have been excluded. It paves the way for the following accurate boundary fitting.

2.3. Eyelids localization

Upper eyelid is often occluded by eyelashes and lower eyelid tends to be of low contrast. Moreover, their boundaries are not as regular as pupillary and limbic boundaries. These facts make eyelids localization more difficult.

As we are only concerned with eyelids which occlude the iris region, the eyelids detection areas are restricted in the rectangles as shown in Figure 4 (a). We first detect candidate eyelids points by Canny detector with low thresholds to ensure almost all valid points are included. And then, the previously learned eyelid boundary detectors are employed to test every candidate points. The points passed the test are processed for further noise removal by: 1) Only one point with maximum $F(x)$ in each column is remained; 2) Isolated points are filtered out. After these steps, remaining points are most valid points. Assuming there are P remaining points for upper or lower eyelid and their positions are denoted in column and row coordinates as $(c_1, r_1), \dots, (c_p, r_p), \dots, (c_P, r_P)$. We model the eyelids as parabolas:

$$f(c) = \kappa(c - v_c)^2 + v_r, \quad (6)$$

where κ affects the parabola's curvature, (v_c, v_r) denotes the vertex. Parabolas' parameters can be solved by minimizing the least squares error. However, a few noisy points may still exist due to complex texture of iris or eyelashes (see Figure 4 (c) for example). These outliers impact the least squares fitting seriously. Therefore, we apply the robust

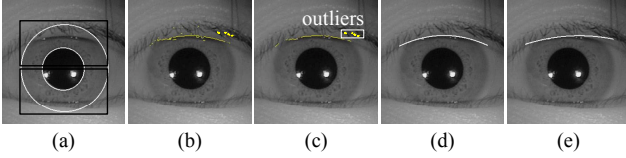


Figure 4. Eyelids localization (better viewed in color). (a) Localized pupillary and limbic boundaries. The black rectangles denote the regions for upper and lower eyelids localization. (b) Yellow pixels are detected by the learned upper eyelid detector; (c) Eyelids points after further noise removal; (d), (e) The upper eyelid is fitted as a parabola by robust least squares fitting or least squares fitting respectively.

least squares fitting to solve the parameters:

$$\min_{\kappa, v_c, v_r} \sum_p w_p (r_p - f(c_p))^2, \quad (7)$$

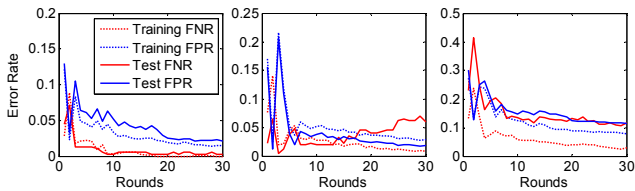
where w_p varies with the residual $re_p = r_p - f(c_p)$ as a Cauchy function:

$$w_p = \frac{1}{1 + (re_p/t)^2}, \quad (8)$$

where t is a constant set according to applications. It gives small weights to noisy outliers which are far from the boundary. As a result, fitting results will be more robust.

Figure 4 shows the intermediate results in upper eyelid localization. Because some outliers existed on the right eyelashes in (c), fitted upper eyelid in (e) is somewhat upswept.

3. Experimental results



(a) Left pupillary boundary (b) Left limbic boundary (c) Upper eyelid boundary

Figure 5. Classification error rates of different boundary detectors in training sets and test sets vs. number of weak classifiers.

Experiments are carried out on CASIA-Iris-Thousand database [1] to evaluate the effectiveness of the proposed method. The database includes 20,000 iris images from 2,000 eyes of 1,000 persons. Because a large number of subjects wore glasses during image capture, many iris images in the database are with large specular reflections and glasses frames (Figure 1 shows some examples) that make iris segmentation particularly difficult.

3.1. Boundary detectors training

We manually labeled 50 images which are randomly selected from the first 25 eyes in CASIA-Iris-Thousand database. Then training data are sampled from the labeled pixels. The patch size is set to 17×17 experimentally. The training set is only a small subset of the whole database.

To determine the number of features used in the later detection procedure, we divide labeled samples into a training set (about 8,000 samples) and a test set (about 2,000 samples) for each detector. The False Positive Rate (FPR) and False Negative Rate (FNR) curves of left pupillary, left limbic and upper eyelid boundary detectors are shown in Figure 5 (error rates for other three detectors are similar). According to the error rates, we choose 20 features for pupillary boundary and eyelids detection, and 12 features for limbic boundary detection.

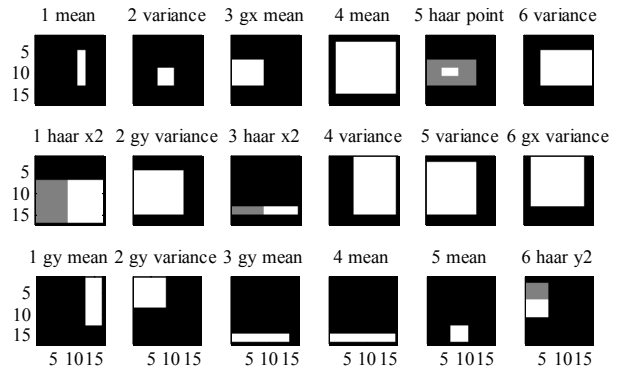


Figure 6. Top, middle and bottom rows are the first six features of left pupillary, left limbic and upper eyelid boundary detectors selected by Gentle AdaBoost, respectively. The patch size is 17×17 with black regions as backgrounds. gx and gy denote features extracted from the horizontal or vertical gradient image.

Figure 6 shows the first six features for left pupillary, left limbic and upper eyelid boundaries detection selected by Gentle AdaBoost (selected features for other three detectors are similar). In the top row, we observe that intensity information is primarily important for pupillary boundary detection since pupils are usually dark in near infrared iris images. Textures and gradients in the horizontal direction are also useful because rich iris textures are often around a pupil and their gradients are high. The selected haar point feature is due to spots near the pupillary boundary. For left limbic boundary detection in the middle row, because intensities change gradually around the boundary, haar-like features in the horizontal direction, gray variance and gradient variance are selected. Moreover, the sizes of the selected features for limbic boundary detection tend to be larger than that for pupillary and eyelids boundaries. In the bottom row, on account of eyelashes and shadows around the upper eyelid, gradient and intensity features are selected. The haar-

like feature in the vertical direction describes the fact that the intensity of a eyelid boundary is generally lower than the intensity in iris regions.

3.2. Localization performance

We compare our Learned Boundary Detectors (LBD) based segmentation method with the state-of-the-art method proposed by He *et al.* [8]. To illustrate the effect of weights used in Hough transforms, we also compare weighted Hough transforms with Hough transforms without weights.

In order to state conveniently, we will use some abbreviations of different segmentation methods in the rest of the section. Each abbreviation is described as follows:

He_PP: Pupillary and limbic boundaries are localized by the Pulling and Pushing method (PP) proposed by He *et al.* [8].

He_PP+EL: Eyelids are localized by the method described in [8] after *He_PP*.

LBD_noHW: Pupillary and limbic boundaries are localized by LBD based method. Hough transforms without weights are used to determine the parameters of iris rings.

LBD_HW: Weighted Hough transforms are used to determine the parameters of iris rings.

LBD_HW+EL: Eyelids are localized by the proposed eyelids localization method after *LBD_HW*.

To evaluate the pupillary and limbic boundaries localization accuracy of each method, we first create benchmarks of pupillary and limbic boundaries manually on the whole database. As the boundaries are modeled as circles, a benchmark for an iris image can be denoted as $(O_{pBen}, R_{pBen}, O_{lBen}, R_{lBen})$ which means the center and the radius of the pupil, the center and the radius of the limbus respectively. Given one algorithm generates a localization result $(O_{pAlg}, R_{pAlg}, O_{lAlg}, R_{lAlg})$ for the same image, we then calculate the localization difference rate DR between the result obtained by the algorithm and the benchmark by:

$$DR = \begin{cases} DR_t & \text{if } DR_t \leq 1 \\ 1 & \text{otherwise} \end{cases}, \quad (9)$$

where:

$$DR_t = \max\{DR_{Op}, DR_{Rp}, DR_{Ol}, DR_{Rl}\}, \quad (10)$$

in which:

$$DR_{Op} = \|O_{pAlg} - O_{pBen}\|_2 / R_{pBen}, \quad (11)$$

$$DR_{Rp} = |R_{pAlg} - R_{pBen}| / R_{pBen}, \quad (12)$$

$$DR_{Ol} = \|O_{lAlg} - O_{lBen}\|_2 / R_{lBen}, \quad (13)$$

$$DR_{Rl} = |R_{lAlg} - R_{lBen}| / R_{lBen}. \quad (14)$$

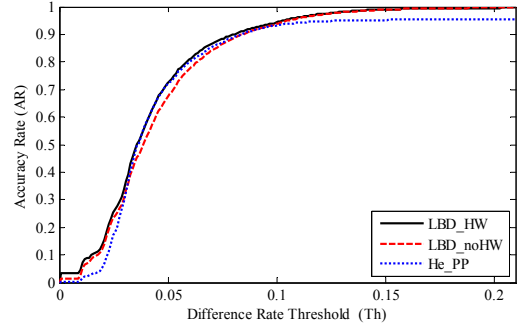


Figure 7. Accuracy rate vs. difference rate threshold on CASIA-Iris-Thousand database.

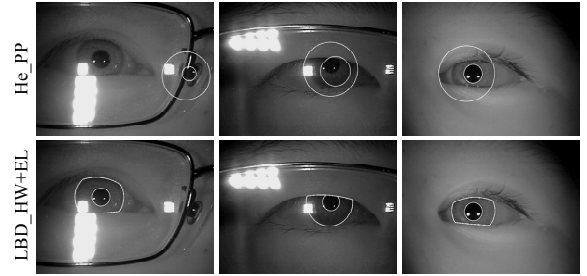


Figure 8. Examples of segmentation results. From Top to Bottom: Segmentation results by *He_PP* [8] and *LBD_HW+EL*.

The DR is normalized by radiuses for size invariant and cut to 1 when it is greater than 1 because a totally miss localization occurs. The DR provides a comprehensive evaluation for pupillary and limbic boundaries localization considering both positions and radiuses.

The accuracy rate AR of pupillary and limbic boundaries localization is defined according to the DR :

$$AR(DR \leq Th) = \frac{\sum_{n=1}^N \delta(DR_n \leq Th)}{N}. \quad (15)$$

where DR_n is the DR for the n -th image, Th is a threshold, N is the total number of tested images. The accuracy rate curves varying with the Th are shown in Figure 7. *LBD_HW* achieves slightly better results than *He_PP*'s and *LBD_noHW*'s when $Th < 0.1$. As $Th > 0.1$, *LBD_HW* and *LBD_noHW* achieve comparable results which are better than *He_PP*'s.

The top row in Figure 8 shows some serious localization errors generated by *He_PP*. The edges caused by eyeglass frames, large specular reflections, eyelids and canthuses mislead the localization. Segmentation results in the bottom row illustrate the robustness of our method.

Figure 9 shows more detailed localization results. Noises created by eyelashes may still influence *He_PP+EL* even though horizontal rank filtering and histogram filtering have

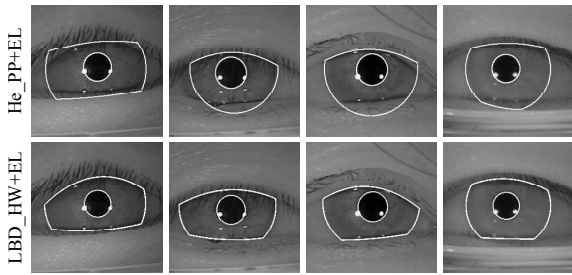


Figure 9. Additional examples of segmentation results. From Top to Bottom: Segmentation results by *He_PP+EL* [8] and *LBD_HW+EL*.

been adopted before eyelids fitting. *LBD_HW+EL* obtains better fine localization results for blurry and noisy boundaries.

We implement our algorithm by MATLAB and run it in a PC with 2.4 GHz CPUs. The average time cost per iris segmentation is about 4.2s, which is slower than *He_PP+EL*. In a word, the proposed method improves the segmentation accuracy at the cost of speed.

4. Discussions and conclusions

In this paper, we have presented a robust iris segmentation method based on learned boundary detectors. There are three major contributions. Firstly, we construct class-specific boundary detectors for iris boundary detection by Gentle AdaBoost. The detectors pave the way for the following iris segmentation procedures. Secondly, we use the output of detectors as the voting weight in Hough transforms to get more stable results. We further constrain the voting angle ranges as we have known approximate position relations between the detected boundary points and the center. Thirdly, eyelids are fitted as parabolas by robust least squares fitting which are much less sensitive to outliers. Extensive experiments on the challenging CASIA-Iris-Thousand iris image database have shown the proposed method achieves state-of-the-art iris segmentation accuracy.

The proposed method can be improved further. The speed can be accelerated by designing more efficient features and classifiers. We currently model the pupillary and limbic boundaries as circles. However, the boundaries are hard to be fitted as circles in some cases (*e.g.* off-angle eyes). Therefore, more elastic models will be considered in our future work.

Acknowledgements: This work is funded by the National Basic Research Program of China (Grant No. 2012CB316300), National Natural Science Foundation of China (Grant No. 60736018, 61075024, 61103155), International S&T Cooperation Program of China (Grant No. 2010DFB14110) and National Key Technology R&D Program (Grant No. 2012BAK02B01).

References

- [1] CASIA Iris Image Database. <http://biometrics.idealtest.org/>.
- [2] P. Arbeláez, M. Maire, C. Fowlkes, and J. Malik. Contour detection and hierarchical image segmentation. *IEEE Trans. on PAMI*, 33(5):898–916, May 2011.
- [3] J. Canny. A computational approach to edge detection. *IEEE Trans. on PAMI*, 8(6):679–698, Nov. 1986.
- [4] J. Daugman. High confidence visual recognition of persons by a test of statistical independence. *IEEE Trans. on PAMI*, 15(11):1148–1161, Nov. 1993.
- [5] J. Daugman. How iris recognition works. *IEEE Trans. on CSVT*, 14(1):21–30, Jan. 2004.
- [6] P. Dollár, Z. Tu, and S. Belongie. Supervised learning of edges and object boundaries. In *Proc. of CVPR*, volume 2, pages 1964–1971, 2006.
- [7] J. Friedman, T. Hastie, and R. Tibshirani. Additive logistic regression: a statistical view of boosting. *The Annals of Statistics*, 28(2):337–374, 2000.
- [8] Z. He, T. Tan, Z. Sun, and X. Qiu. Toward accurate and fast iris segmentation for iris biometrics. *IEEE Trans. on PAMI*, 31(9):1670–1684, Sept. 2009.
- [9] V. Jain, B. Bollmann, M. Richardson, D. Berger, M. Helmstaedter, K. Briggman, W. Denk, J. Bowden, J. Mendenhall, W. Abraham, K. Harris, N. Kasthuri, K. Hayworth, R. Schalek, J. Tapia, J. Lichtman, and H. Seung. Boundary learning by optimization with topological constraints. In *Proc. of CVPR*, pages 2488–2495, June 2010.
- [10] R. Lienhart and J. Maydt. An extended set of haar-like features for rapid object detection. In *Proc. of ICIP*, volume 1, pages 900–903, 2002.
- [11] X. Liu, K. Bowyer, and P. Flynn. Experiments with an improved iris segmentation algorithm. In *Fourth IEEE Workshop on Automatic Identification Advanced Technologies*, pages 118–123, Oct. 2005.
- [12] X. Liu, P. Li, and Q. Song. Eyelid localization in iris images captured in less constrained environment. In *Proc. of ICB*, pages 1140–1149, 2009.
- [13] H. Proença and L. Alexandre. Iris segmentation methodology for non-cooperative recognition. *IEE Proc. of Vision, Image and Signal Processing*, 153(2):199–205, April 2006.
- [14] S. Shah and A. Ross. Iris segmentation using geodesic active contours. *IEEE Trans. on IFS*, 4(4):824–836, Dec. 2009.
- [15] A. Shahrokni, T. Drummond, F. Fleuret, and P. Fua. Classification-based probabilistic modeling of texture transition for fast line search tracking and delineation. *IEEE Trans. on PAMI*, 31(3):570–576, March 2009.
- [16] R. Tang and S. Weng. Improving iris segmentation performance via borders recognition. In *Proc. of ICICTA*, volume 2, pages 580–583, 2011.
- [17] A. Torralba, K. Murphy, and W. Freeman. Sharing features: efficient boosting procedures for multiclass object detection. In *Proc. of CVPR*, volume 2, pages 762–769, 2004.
- [18] R. Wildes. Iris recognition: an emerging biometric technology. *Proc. of the IEEE*, 85(9):1348–1363, Sept. 1997.
- [19] X. Zhang, Z. Sun, and T. Tan. Texture removal for adaptive level set based iris segmentation. In *Proc. of ICIP*, pages 1729–1732, Sept. 2010.